Applied Catalysis B: Environmental 179 (2015) 106–112

Contents lists available at ScienceDirect

Applied Catalysis B: Environmental

journal homepage: www.elsevier.com/locate/apcatb

Enhanced visible-light-driven photocatalytic removal of NO: Effect on layer distortion on g-C_3N_4 by H_2 heating

Wingkei Ho[a,c,*], Zizhong Zhang[a,b,*], Mukun Xu[b], Xianwen Zhang[b], Xuxu Wang[b], Yu Huang[c]

[a] Department of Science and Environmental Studies, The Hong Kong Institute of Education, Hong Kong, China
[b] Research Institute Photocatalysis, State Key Laboratory of Photocatalysis on Energy and Environment, Fuzhou University, Fuzhou 350002, China
[c] Key Lab of Aerosol Chemistry & Physics and State Key Lab of Loess and Quaternary Geology, Institute of Earth Environment, Chinese Academy of Sciences, Xi'an 710075, China

ARTICLE INFO

Article history:
Received 21 January 2015
Received in revised form 4 April 2015
Accepted 6 May 2015
Available online 7 May 2015

Keywords:
g-C_3N_4
Layer distortion
H_2 heating
NO removal
Photocatalysis

ABSTRACT

We report a simple strategy for realizing the tunable structure distortion of graphitic carbon nitride (g-C_3N_4) layers by H_2 post calcination to improve the intrinsic electronic structure and the photocatalytic performances of g-C_3N_4 samples. In comparison with the O_2 or N_2 post treatment, the H_2-modified g-C_3N_4 develops new optical absorption above 460 nm and enhances photocatalytic activity for NO removal. The combined characterization results reveal that H_2 heating induced the structure distortion of g-C_3N_4 layers is originated from the creation of amino groups within the structure and generation of the strong hydrogen bonding interactions between layers. The distorted structure allows n–π^* electron transitions in g-C_3N_4 to increase visible-light absorption. The structure distortion also enables more electrons to be available for initiating the photocatalytic reaction and the separation of photogenerated charge carriers in g-C_3N_4. This work provides a simple strategy for realizing the tunable structure distortion of g-C_3N_4 layers to adjust its electronic structure and photocatalysis.

1. Introduction

State-of-the-art band gap engineering is a complex but powerful technique for tailoring the electronic structure of semiconductors, thereby achieving the control of conductive, optical, or other physical properties for targeted applications [1–3]. Many inorganic semiconductor photocatalysts have been successfully advanced to narrow their energy gap for visible light harvesting and adjusting the redox potentials of photo-induced charge carriers for relevant chemical conversions by band gap engineering through altering the compositions of photocatalysts [4]. This advancement opens the door to exciting possibilities for the design of photocatalytic materials for efficient solar energy conversion.

Recently, graphitic carbon nitride (g-C_3N_4) has attracted considerable interests as a fascinating metal-free and visible-light-driven photocatalyst for the direct conversion of sustainable solar energy to chemical energy and is finding new applications in H_2 production, environmental purification, organic photosynthesis, and CO_2 reduction [5–8]. However, bulk g-C_3N_4 photocatalysts are still seriously suffering from many drawbacks, mainly including low quantum efficiency and the lack of absorption above 460 nm [9], which inevitably limit their further applications. Thus, control to modulate the intrinsic electronic structures and solar light harvesting of g-C_3N_4 system is specifically requested to maximize the photocatalytic performance.

The bulk g-C_3N_4 is a conjugated organic polymer that is able to combine plastic electronics and optoelectronics with easy processability. The organic nature of g-C_3N_4 allows plentiful organic schemes to be utilized to engineer the molecular structure, electronic structure, and texture. Thus, the chemical synthesis of g-C_3N_4 can be directly integrated with various physical and chemical methods, including nanocasting [10], elemental doping [11], and copolymerization [12], to adjust the chemical composition, texture, electronic structure, and the photocatalytic behavior of g-C_3N_4. For example, S-doped or Zn-doped g-C_3N_4 prepared by a simple soft-chemical method has displayed a good photocatalytic activity for H_2 production under visible light illumination [13]. A high-surface area g-C_3N_4 with mesoporous nanostructure can be easily prepared by the polymerization of cyanamide on a silica template [14]. Thiophene derivative or barbituric acid monomers can be chemically incorporated into the conjugated polymeric network of g-C_3N_4 and extend the optical absorption edge of g-C_3N_4 to lower

* Corresponding author. Tel.: +852 29488255.
E-mail addresses: keithho@ied.edu.hk (W. Ho), z.zhang@fzu.edu.cn (Z. Zhang).

http://dx.doi.org/10.1016/j.apcatb.2015.05.010
0926-3373/

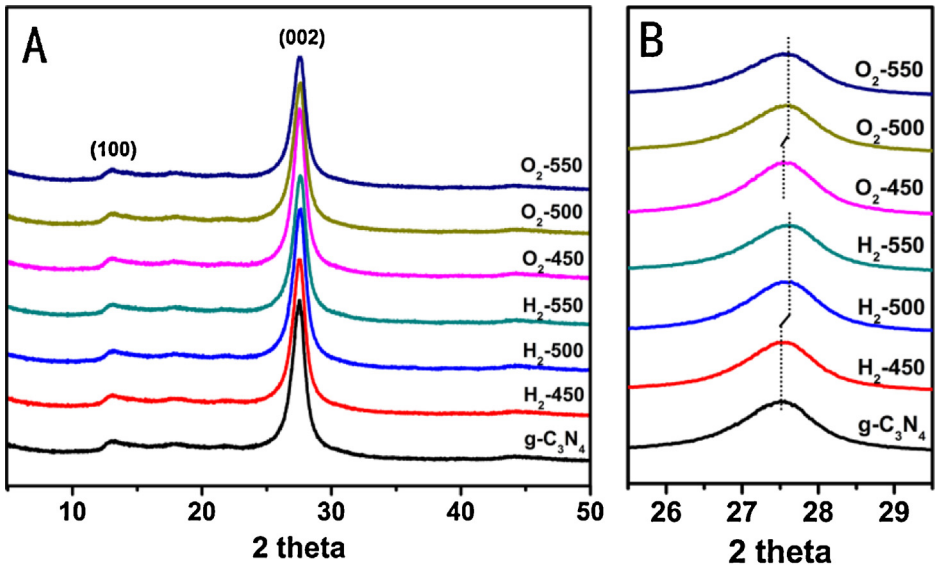

Fig. 1. XRD patterns of the g-C_3N_4 samples.

energy [15,16]. These strategies not only promote the photocatalytic activity of g-C_3N_4 but also offer the possibility for further modification of g-C_3N_4 with sensitizers and co-catalysts. However, developing a simple approach to improve the intrinsic electronic structures and photocatalytic properties of g-C_3N_4 is still desirable.

Perfect g-C_3N_4 is constructed from N-bridged "poly(tri-s-triazine)" to form π-conjugated graphitic plane with weak van der Waals interaction between layers. The electronic structure of g-C_3N_4 is related to sp^2 hybridization of carbon and nitrogen that forms π-conjugated graphitic planes. The visible-light-response of the photocatalyst originates from an electron transition from the valence band populated by N2p orbitals to the conduction band formed by C2p orbitals. Accordingly, the band gap energy of g-C_3N_4 sensitively depends on the degree of condensation and the packing between the layers, and the photocatalytic efficiency of g-C_3N_4 seriously relies on the excited electrons from N2p orbitals. Therefore, tuning the degree of condensation and the electrons of the N2p involved in π-conjugated system is an alternative way to improve the intrinsic electronic structures and photocatalytic performance of g-C_3N_4. Increasing the degree of polymerization by increasing condensation temperature has been proved to linearly decrease the bandgap of g-C_3N_4 from 3.0 eV to 2.5 eV [17]. To our knowledge, a few works have considered the electrons of the N2p involved in π-conjugated system for tuning the intrinsic electronic structures and improving the photocatalytic activity of g-C_3N_4.

In this work, we developed a simple approach to improving visible optical absorption and the photocatalytic activity of g-C_3N_4 using H_2 heating treatment. For the comparison, the effect of H_2 or O_2 or N_2 heating treatment on the structure of g-C_3N_4 was characterized in detail by elemental analysis (EA), UV–vis spectroscopy, FTIR, XPS, solid-state NMR, and EPR. NO removal was used as a model reaction to examine the visible light photocatalytic reactivity of modified g-C_3N_4 catalysts. We demonstrated that only H_2 heating induces the structure distortion of g-C_3N_4 layers that results in considerable electrons from the edge N2p involved in π-conjugated system to narrow the band gap and improve the photocatalytic performance of g-C_3N_4.

2. Experimental

2.1. Sample preparation

The parent g-C_3N_4 powder was synthesized typically by heating 15 g of melamine in a semi-closed alumina crucible with a cover under helium gas flow (60 mL/min) to 550 °C for 4 h at a heating rate of 5 °C min^{-1}, followed by naturally cooling to room temperature. The product was collected and ground into powder.

The modified g-C_3N_4 was prepared by heating the parent g-C_3N_4 powders under H_2 (or O_2) gas flow (60 mL/min) at a rate of 2 °C min^{-1} to 450, 500, or 550 °C for 3 h. The modified samples were denoted as g-C_3N_4-H_2-X or g-C_3N_4-O_2-X, where X refers to heating temperature.

2.2. Characterization

C, N, and H contents were measured on an Elementar Vario EL analyzer. X-ray diffraction (XRD) measurements were performed on a Bruker D8 Advance X-ray diffractometer using CuKα_1 radiation (λ = 1.5406 Å). BET measurements were conducted using a Micrometrics ASAP 2020 surface area/porosity analyzer. UV–vis spectra were recorded on a Varian Cary 500 Scan UV–vis–NIR spectrophotometer using a $BaSO_4$ standard. FTIR spectra were obtained using a Nicolet Magna 670 FTIR spectrometer with a DTGS detector. EPR spectra were recorded at room temperature by a Bruker A-300-EPR X-band spectrometer. XPS spectroscopy was conducted on a VG ESCALAB 250 XPS system with a monochromatized Al Ka X-ray source (15 kV, 200 W, 500 μm pass energy = 20 eV). All binding energies were referenced to the C1s peak at 284.6 eV of surface adventitious carbon. Solid-state ^{13}C NMR spectra were recorded using a Bruker Advance III 500 spectrometer.

Table 1
BET specific surface area and pore volume of the g-C_3N_4 samples.

Samples	g-C_3N_4	H_2-450	H_2-500	H_2-550	O_2-450	O_2-500	O_2-550
BET (m^2/g)	13.8	11.2	15.8	28.0	14.5	18.1	22.6
Pore volume (cm^3/g)	0.063	0.059	0.083	0.157	0.069	0.080	0.112

Table 2
Bulk C, N, and H contents in the g-C_3N_4 samples by EA.

Samples	N[%]	C[%]	H[%]	C:N	H:N
g-C_3N_4	61.12	35.13	1.716	0.671	0.393
O_2-550	60.79	34.98	1.728	0.671	0.398
H_2-550	60.74	34.96	1.765	0.671	0.407

2.3. Photocatalytic measurements

The photocatalytic activity was measured by NO removal at approximately 600 ppb levels in a continuous flow reactor at ambient temperature (shown in Fig. S1). The volume of the rectangular reactor, which is made of stainless steel and covered with quartz glass window, was 4.5 L (30 cm × 15 cm × 10 cm). A 30 W visible LED (the light spectra of LED shown in Fig. S2) as a light source was vertically placed outside the reactor. Photocatalyst (0.2 g) was coated onto a dish with a diameter of 12.0 cm. The coated dish was pretreated at 70 °C to remove water in the suspension. NO gas was acquired from a compressed gas cylinder at a concentration of 50 ppm of NO (N_2 balance) and diluted to approximately 600 ppb by using a dynamic gas calibrator (Ecotech GasCal 1000) in combination with a zero air supply. The gas flow rate through reactor was controlled at 1000 mL/min by a mass flow controller. After the adsorption–desorption equilibrium was achieved, the lamp was turned on. The concentration of NO was continuously measured using a NOx analyzer model T200 (Teledyne API). The removal ratio (δ) of NO was calculated as $\delta(\%) = (1 - C/C_0) \times 100\%$, where C_0 is the initial concentration of NO, and C is the concentration of NO after photocatalytic reaction.

3. Results

3.1. Structural characteristics

The XRD patterns of the pristine and modified g-C_3N_4 are displayed in Fig. 1. Typically, two individual well-resolved peaks can be determined for the pristine g-C_3N_4. The strong peak at 27.5° corresponding to an interplanar distance of approximately 0.324 nm was characterized for (002) reflection of graphitic layered materials, whereas the weak one at 13.0° (d = 0.680 nm) for (100) reflection can be attributed to the in-plane structural packing motif of tri-s-triazine units. Upon heating in H_2 or O_2, the graphitic-like structure of g-C_3N_4 was retained without an impurity phase. However, the main peak at 27.5° was slightly shifted to higher angles as the heating temperature increased (Fig. 1B), which reflected a reduction in the stacking distance between layer plane. The post-calcination at 550 °C either in H_2 or in O_2 atmosphere decreased the interplanar distance from 0.324 nm to 0.323 nm. A little bit decrease in the interplanar distance of g-C_3N_4 after both O_2 and H_2 heating is mainly because heating treatment is not enough higher temperature or longer reaction time. The post-calcination caused layer condensation that maybe resulted in structure distortions and consequent semiconductive properties of g-C_3N_4. Moreover, the diffraction peak at 27.5° became weaker for the post-calcination at 550 °C, which also indicated that the large plane of g-C_3N_4 was tailored to small sample sizes, and structure defects were formed. This result was verified by the increase of BET specific surface area and pore volume of g-C_3N_4 samples with increasing post-calcination temperature (Fig. S3 and Table 1). The increased surface area of g-C_3N_4 could provide more reactive sites and enhance light harvesting. The carbon and nitrogen stoichiometry determined by EA (Table 2) showed that the bulk C/N molar ratio was approximately 0.67 with an H_2 content of 1.72% for the pristine g-C_3N_4. The C/N ratio (0.67) of the prepared g-C_3N_4 was lower than the theoretical value (0.75) because of the presence of incomplete condensation amino group, which is consistent with a reported result [18]. The bulk C/N molar ratio was not changed after the thermal treatment in either H_2 or O_2 atmosphere. However, the H content or H/N molar ratio was obviously increased by H_2 heating, as compared with that in the pristine g-C_3N_4 samples or by O_2 heating. This result implied that H_2 heating induced H atoms blended into g-C_3N_4 structure and possibly formed more amino group presence in samples.

3.2. Optical properties

Fig. 2 compares the optical absorption spectra of the pristine and modified g-C_3N_4. The pristine g-C_3N_4 showed a sharp absorption edge of 456 nm, which corresponded to a band gap of 2.72 eV. After the modification in H_2, a broad absorption shoulder above 460 nm tailed the absorption that increased to approximately 700 nm besides the main band edge absorption of g-C_3N_4 at 456 nm. The intensity of the absorption shoulder remarkably increased with heating temperature. The g-C_3N_4-H_2-550 samples exhibited the best ability of visible light absorption. This result suggested that a facile way by post-calcination in H_2 can greatly improve the ability of g-C_3N_4 to harvest visible light. By contrast, the post-calcination in O_2 induced not only a broad absorption shoulder above 460 nm but also the shift of absorption edges to longer wavelengths with increasing temperature. For the post-calcination at 550 °C in O_2 atmosphere, the absorption edges shifted to 469 nm (corresponding to 2.64 eV) as compared with 456 nm (2.72 eV) for the pristine g-C_3N_4 samples. However, the absorption shoulder in the 460–700 nm region for H_2 post-calcination was significantly more intense than that for O_2 post-calcination at the same temperature. Moreover, we also investigated the UV–vis spectra of the g-C_3N_4 by the post calcination in N_2 atmosphere at 550 °C, as shown in Fig. S4. Both the red shift and the absorption shoulder were not observed at all for N_2 post calcination. These implied that the mechanism of H_2 heating was different from that of O_2 or N_2 heating to adjust the intrinsic electron structure of g-C_3N_4. Thermal annealing at high temperature has been reported to result in compacting polymeric sheets and narrowing the band gap of g-C_3N_4 [17]. Although both H_2 and O_2 calcination at 550 °C induced the same decrease of interplanar distance from 0.324 nm to 0.323 nm, only the O_2 annealing caused the shift of the intrinsic absorption edges to longer wavelengths. A distinct intrinsic nature existed between H_2 and O_2 post-calcination to improve the optical absorption properties of g-C_3N_4 samples. The feature shoulder absorption above 460 nm can be attributed to n–π^* transitions that involved lone pairs on the edge N atoms of the heptazine rings [19].

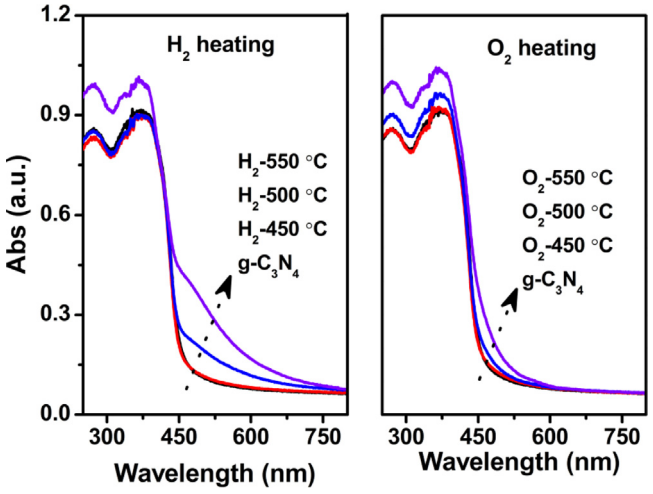

Fig. 2. UV–vis light absorption spectra of the g-C_3N_4 samples.

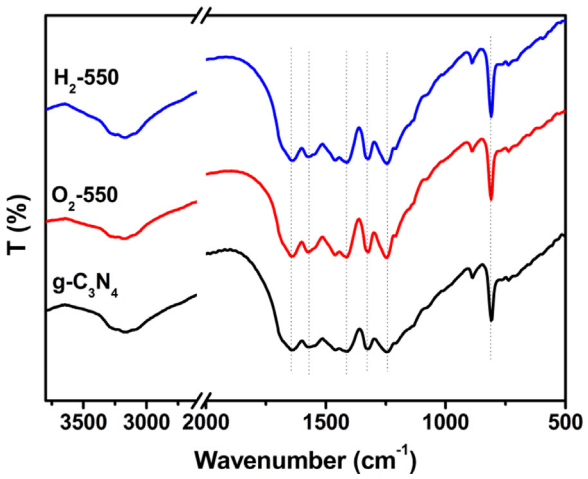

Fig. 3. FT-IR spectra of the g-C_3N_4 samples.

Such transitions were forbidden for perfectly symmetric and planar heptazine units but allowed if the structures were distorted by increasing layer condensation, as confirmed by the above XRD results (Fig. 1). Therefore, H_2 heating maybe results in the structure distortion of g-C_3N_4 and thus allows for n–π^* transitions.

3.3. IR

The FTIR spectra of the pristine and modified g-C_3N_4 are shown in Fig. 3. All FTIR spectra of the as-prepared g-C_3N_4 samples showed multiple bands at 1200–1600 cm^{-1} for the typical aromatic CN heterocycles and the band at 800 cm^{-1} for heptazine units [20]. A series of bands in the region above 3200 cm^{-1} can be assigned to the stretching modes of uncondensed amino groups at the sample surfaces. Besides, no any new bands were observed in IR spectra after the thermal annealing in H_2 or O_2 up to 550 °C. Thus, no O impurities were introduced into heptazine units and no change was observed in the skeleton structure of heptazine units of g-C_3N_4 by heating below 550 °C. This result can be attributed to the high thermal stability against oxidation of g-C_3N_4 samples, as reported to be stable in air up to 550 °C [21]. However, H_2 annealing resulted in the enhancement of the bands at 3200 cm^{-1} for amino groups, which indicated that the bridged N bonds with heptazine units were opened to form amino groups. This result is in a good agreement with the above EA results.

3.4. XPS and NMR

To further evaluate the effect of post-calcination on the molecular structure of heptazine units of g-C_3N_4, the chemical states of C, N, and O in the g-C_3N_4 samples were characterized by XPS techniques, as shown in Fig. 4. The C1s XPS displayed the main core level peak at 288.0 eV ascribed to sp^2 hybridized carbon of the tri-s-triazine rings [22], and a weak peak located at 293.4 eV originating from the presence of a slight amount of sp^2-hybridized C atoms attached to terminal uncondensed amino groups (e.g., —NH_2 and —NH) [23]. The N 1s XPS of the parent g-C_3N_4 can be fitted into several peaks. The main peaks at 398.5, 399.8, and 400.9 were corresponded to N bonded to carbon atoms (C=N—C) of tri-s-triazine rings, the tertiary N in the form of N—$(C)_3$, and amino functional groups (—NH_2 or =NH) [24], respectively. A very weak peak at 404.1 eV of N1s was attributed to charging effects or positive charge localization in heterocycles [6]. A weak O1s energy peak at 532.2 eV was also detected and could be assigned to the adsorbed O_2 [25]. No obvious change in chemical states of either C or N was observed for g-C_3N_4 samples modified by heating in H_2 or O_2. This further confirms that no O impurities from O_2 treatment is incorporated into the skeleton structure of heptazine units of g-C_3N_4 to cause the destruct of g-C_3N_4. The C/N molar ratios estimated from XPS spectra were retained to be 0.73 for all samples.

To ensure no destruction in the heptazine units of g-C_3N_4 by H_2 or O_2 heating, the modified samples were also analyzed by ^{13}C solid-state MAS NMR. The ^{13}C NMR spectrum of the pristine g-C_3N_4 (Fig. 5) exhibited two signals centered at 156.2 and 164.3 ppm, which can be attributed to the resonances for the CN_3 and $CN_2(NH_2)$ groups of the heptazine units [26], respectively. H_2 or O_2 heating did not have any significant effect on the signal shape and chemical shifts of all carbon atoms in heptazine units. This result confirmed the structure stability of g-C_3N_4 samples under H_2 or O_2 heating treatment bellow 550 °C.

3.5. EPR

Photocatalytic processes were closely related to the behavior of photogenerated carriers and the intrinsic electronic structure of a photocatalyst. To determine the possible influence of post-treatment on the photogenerated carriers and the intrinsic electronic structure for g-C_3N_4, we used the sensitive EPR technique to investigate the trapped electrons in samples with or without visible light illumination. Fig. 6 shows the X-band EPR spectra of the samples. We observed in all cases an isotropic single-line EPR spectrum near $g = 2.0031$ with a symmetric line of nearly

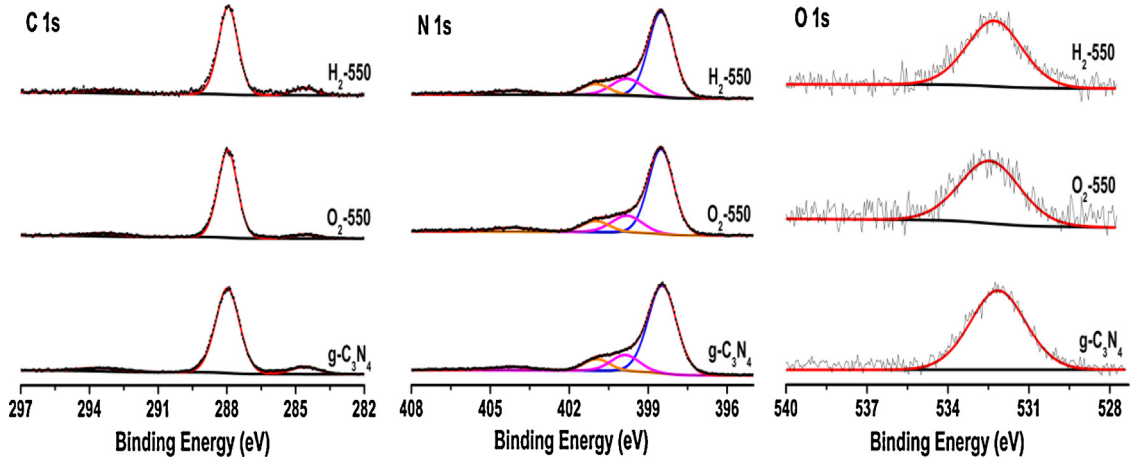

Fig. 4. XPS spectra of the g-C_3N_4 samples.

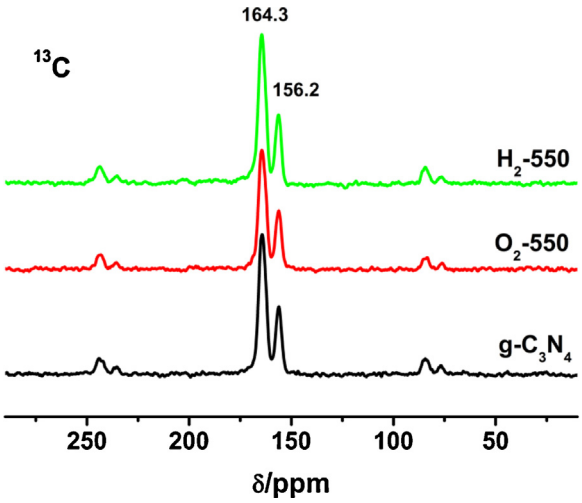

Fig. 5. Solid-state ^{13}C NMR spectra of the g-C_3N_4 samples.

Lorentzian line shape. The intrinsic paramagnetic center arose from the generated conduction electrons in localized π states of g-C_3N_4 [27]. The existence of these conduction electrons will be beneficial for the photocatalytic reactions. The EPR intensities were enhanced significantly after the post-calcination and increased with increasing heating temperature either in H_2 or O_2 atmosphere (Fig. 6C).

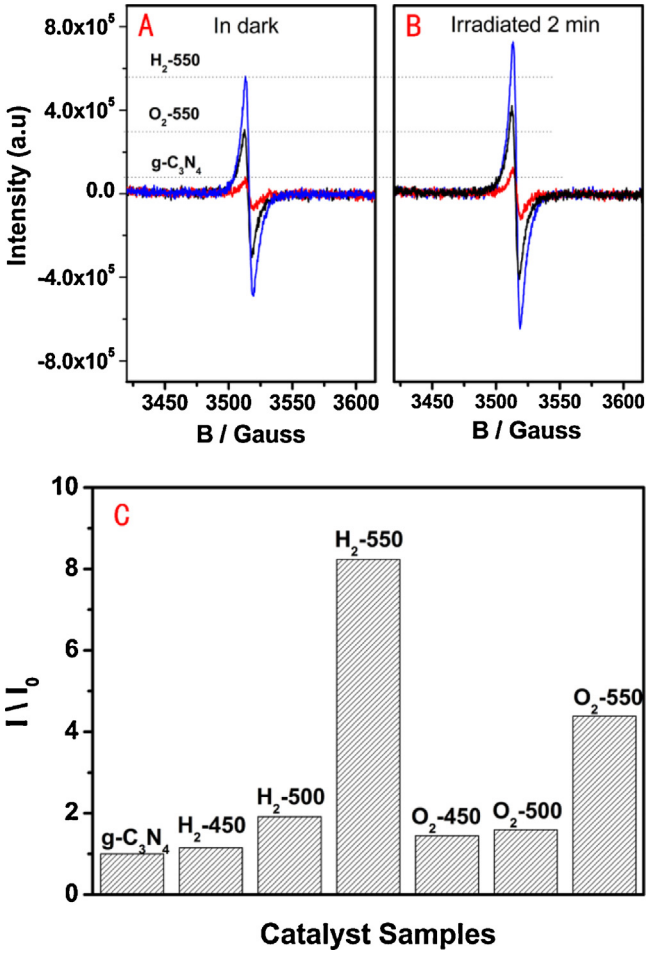

Fig. 6. EPR spectra of the g-C_3N_4 samples in dark (A) and with visible light irradiation (B) measured at room temperature; (C) EPR signal intensity in the pristine and modified g-C_3N_4 samples. I_0 = 1 is the signal intensity in the pristine g-C_3N_4 sample.

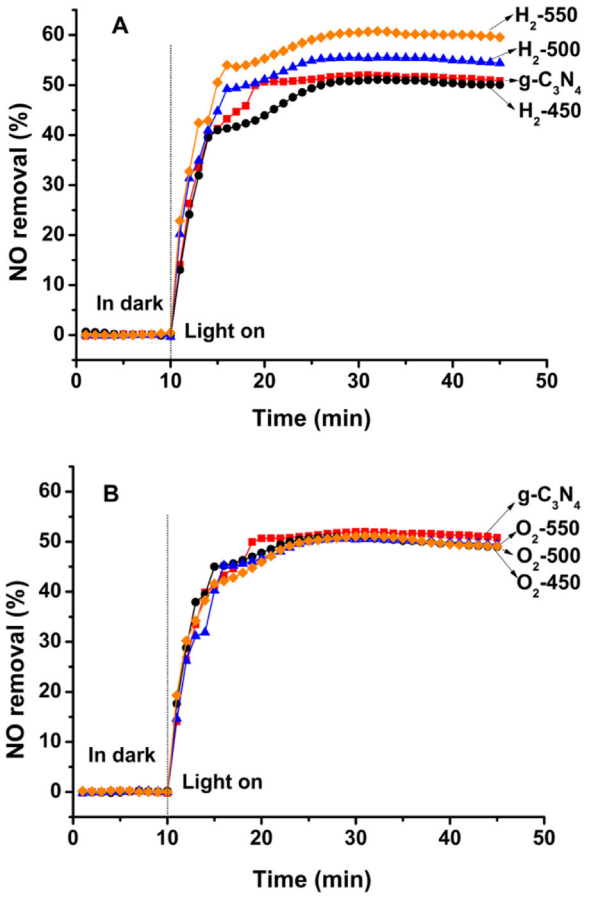

Fig. 7. Time-online data for NO removal over the pristine and modified g-C_3N_4 samples.

For the g-C_3N_4-O_2-550 and g-C_3N_4-H_2-550 samples, the EPR signal increased by a factor of approximately 4.4 and 8.2, respectively. Obviously, H_2 heating was more efficient than O_2 heating to produce the unpaired electrons in localized π system of g-C_3N_4 at the same annealing temperature. Thus, the post-calcination developed a large amount of conduction electrons in g-C_3N_4. The order for the intensity of EPR signal for the modified samples by H_2 or O_2 heating is consistent with their ability of visible light absorption above 460 nm (Fig. 2). When g-C_3N_4 samples were exposed to $\lambda \geq 420$ nm light irradiation for 2 min, the EPR signal can be further increased for the pristine and modified g-C_3N_4 (Fig. 6B) as compared with that for samples in dark (Fig. 6A). This phenomenon indicated the generation of photoexcited electrons in g-C_3N_4 upon absorption of photon, which may be responsible for the photocatalysis of g-C_3N_4-based materials. The enhanced extent of EPR signal with $\lambda \geq 420$ nm light irradiation was in the order of g-C_3N_4-H_2-550 > g-C_3N_4-O_2-550 > g-C_3N_4. This result implied that H_2 heating facilitates the production and separation of photogenerated charge carriers in g-C_3N_4 with visible light illumination, which may lead to higher photocatalytic activity.

3.6. Photocatalytic activity

We used the gas-phase photocatalytic oxidation of NO as a model reaction to evaluate the effect of H_2 and O_2 heating treatments on the photocatalytic behavior of g-C_3N_4 samples under visible LED irradiation. Fig. 7 shows the dependence of the removal of NO on reaction time. For the parent g-C_3N_4 samples, 51.8% removal of NO was obtained at continuous flow system. In the case of samples obtained under H_2 heating treatment, the removal ratio

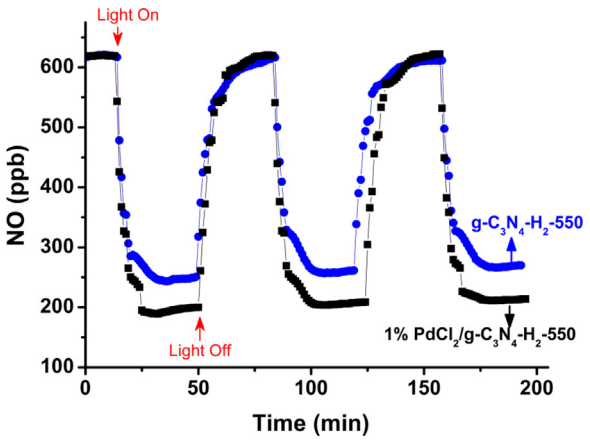

Fig. 8. Stability of the parent and 1% $PdCl_2$ sensitized g-C_3N_4-H_2-550 catalysts.

of NO increased with increasing heating temperature. A maximum removal ratio of 60.7% was reached for H_2 heating at 550 °C (Fig. 7A). By contrast, O_2 heating treatment had no effect on NO removal and was independent of the heating temperature as compared with the pristine g-C_3N_4 (Fig. 7B). Although both H_2 and O_2 induced the similar textural properties of g-C_3N_4, only H_2 treatment increased the NO removal when we compared with heating treatment at same temperature. This indicates that the intrinsic semiconductor properties of g-C_3N_4 are improved by H_2 heating treatment, hence contributing to its enhanced photocatalytic activity, which will be discussed in more detail later in the discussion.

The stability of a catalyst is also important for its application. Fig. 8 displays the prolonged run experiments for NO removal over the optimized g-C_3N_4-H_2-550 catalysts under visible LED illumination. After the photocatalytic reaction for three runs, only slight deactivation of the reaction system occurred, indicating that the modified catalysts were rather stable. The stability of the g-C_3N_4-H_2-550 was further confirmed by FT-IR spectra after the prolonged runs (Fig. S5). Moreover, the activity of the modified g-C_3N_4 catalysts for NO removal can be further improved remarkably by loading with $PdCl_2$ sensitizer. $PdCl_2$ sensitized g-C_3N_4-H_2-550 catalysts (1%) exhibited as high as 69.5% NO removal and a good photocatalytic stability (Fig. 8).

4. Discussion

Either H_2 or O_2 or N_2 post-calcination at high temperature leads to an increase in surface area for the g-C_3N_4 photocatalysts. However, H_2 or O_2 heating treatment induced the optical absorption properties in visible light region and the activity of the modified g-C_3N_4 are distinct from each other. Only the H_2 annealing not only extends the optical absorption up to 460 nm but also enhances photooxidation activity compared with the pristine or O_2 heated g-C_3N_4 samples. Therefore, the changes of texture properties for the modified g-C_3N_4 by heating treatment are not the crucial factor that affects photocatalytic performance. The origin of these phenomena is related to the alternation of the planar structure and the intrinsic electronic structure of g-C_3N_4 by H_2 heating.

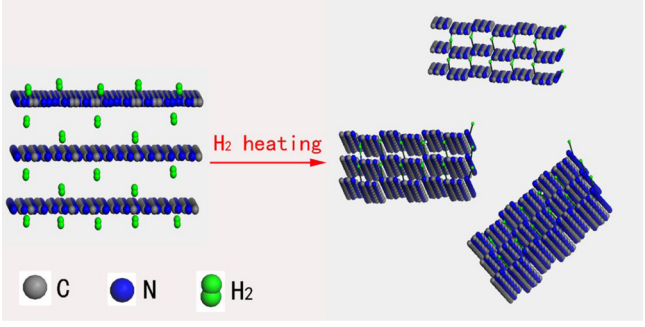

Scheme 1. The proposal mechanism of H_2 heating for the layer distortion of g-C_3N_4.

EA shows that the H/N molar ratio in g-C_3N_4 is increased by H_2 heating, but O_2 heating has no significant effect on the composition of g-C_3N_4. IR and XPS spectra confirm that more amino groups are formed by H_2 heating. The ^{13}C solid-state NMR indicates that the molecular structure and chemical states of heptazine units are not altered by H_2 heating. Based on the results of EA, IR, XPS, and NMR characterization, it confirms that H_2 heating treatment induces H atoms to blend to the bridged N to form amino groups within g-C_3N_4 and tailor the large plane of g-C_3N_4 into small sizes. A reasonable postulation can be made that the smaller size and higher activity of H atom than O atom access easily the space among layers and react with skeleton atoms in g-C_3N_4. Moreover, H atoms introduced into the g-C_3N_4 network preferentially bond with N atoms. However, the heptazine units in g-C_3N_4 are not broken because of the extraordinary stability of heptazine unit with aromaticity properties. The formation of amino groups can result in structure distortions and consequent semiconductive properties of g-C_3N_4.

The distorted structure by thermal condensation of g-C_3N_4 has been indicated by several authors [19,28], which allows n–π^* electron transitions with the appearance of new absorption above 460 nm. Both O_2 and H_2 post treatment at same 550 °C develop the same decrease of interplanar distance for the structure distortion of g-C_3N_4, but only H_2 treatment displays significant absorption above 460 nm. This indicates that H_2 heating is more efficient to develop the distorted structure of g-C_3N_4. The creation of amino groups by H_2 heating maybe account for the distortion, because amino groups facilitates the strong interaction between layers through the hydrogen bonding interactions. The bond length of N—H for amino group is about 0.1 nm, which is much less than the 0.324 nm distance of g-C_3N_4 interplanar layers. The development of amino groups between interplanar layers is completely possible and thus the hydrogen bond. With the formation of more amino groups with increasing heating temperature, the stronger interaction among layers leads to the distortion of planar structure of g-C_3N_4. Such structure distortion results in lone pairs on the edge N atoms of the heptazine rings involved in π-conjugated system that forms n–π^* transitions, which induces higher electron density in π-conjugated system of g-C_3N_4 and conduction electrons in localized π states of g-C_3N_4. It is confirmed by the facts that an additional absorption shoulder in the visible light region above 460 nm (Fig. 2) and an increase in EPR signal (Fig. 6) that corresponds to unpaired electrons in localized π system was observed with increasing H_2 heating temperature. Therefore, H_2 heating treatment is a more efficient approach for layer distortion and improving the ability of g-C_3N_4 to harvest visible light than O_2 or N_2 heating treatment.

The creation of amino group within the structure by H_2 heating may contribute to the highly efficient generation of charged carriers and the high photocatalytic activity of g-C_3N_4. H_2 heating develops the distortion structure and n–π^* transitions to make more electrons involved in π-conjugated system. Such electrons are available for exciting to conduction band to initiate the photocatalytic reaction on g-C_3N_4 surface, as indicated by the significant enhancement of EPR signal with increasing H_2 heating temperature and with visible light irradiation. Although thermal condensation can also lead to enhanced visible light absorption and structure distortion [29], given that we post-calcinate the g-C_3N_4 samples in O_2 atmosphere in this study, such thermal condensation treatment has no significant effect on the photocatalytic activity of g-C_3N_4 toward NO removal (Fig. 7B). Moreover, H atom introduced into g-C_3N_4 benefits the separation of photogenerated charge carriers because

H atoms are electron-deficient and may serve as an electron sink [30]. Therefore, H_2 heating is a simple but efficient strategy to realize tunable optical properties and photocatalysis of g-C_3N_4 , as shown in Scheme 1.

5. Conclusions

The intrinsic optical properties and photocatalytic activity of g-C_3N_4 are significantly improved through a simple but efficient strategy by H_2 post calcination. The modified g-C_3N_4 shows an additional absorption shoulder in the visible light region above 460 nm and more amino groups created within the structure but no change in heptazine units of g-C_3N_4 polymer compared with pristine g-C_3N_4 samples. The combined characterization results reveal that the creation of amino groups within the structure by H_2 heating efficiently induces the distortion of planar structure of g-C_3N_4. Such distortion forms n–π^* transitions to narrow the band gap energy for more visible light harvesting. The n–π^* transitions and distortion structure result in more electrons available for initiating the photocatalytic reaction and benefits the separation of photogenerated charge carriers to improve the photocatalytic properties of g-C_3N_4. In summary, this study develops an alternative way to develop the distorted structure of g-C_3N_4 for improving the intrinsic electronic structures and photocatalytic performance.

Acknowledgments

This research was financially supported by the research grant of Early Career Scheme (ECS 809813) from the Research Grant Council, Hong Kong SAR Government, Dean's Research Fund-Early Career Researchers (04022), Research Equipment Grant (REG-2), and Internal Research Grant (R3429) from The Hong Kong Institute of Education. This work was also financially supported by the NSFC (Grant Nos. 21203029 and U1305242), National Basic Research Program of China (973 Program, No. 2014CB260410) and the Natural Science Foundation of Fujian Province of PR China (2013J05024), and Technology Project of Education Office of Fujian Province of PR China (JA12036).

Appendix A. Supplementary data

Supplementary data associated with this article can be found, in the online version, at http://dx.doi.org/10.1016/j.apcatb.2015.05.010

References

[1] W. Yin, S. Wei, M.M. Al-Jassim, Y. Yan, Phys. Rev. Lett. 106 (2011) 066801.
[2] P.D. Tran, L.H. Wong, J. Barber, J.S.C. Loo, Energy Environ. Sci. 5 (2012) 5902–5918.
[3] W. Zhou, Y. Liu, Y. Yang, P. Wu, J. Phys. Chem. C 118 (2014) 6448–6453.
[4] D. Lehr, M. Luka, M.R. Wagner, M. Bügler, A. Hoffmann, S. Polarz, Chem. Mater. 24 (2012) 1771–1778.
[5] X. Wang, K. Maeda, A. Thomas, K. Takanabe, G. Xin, J.M. Carlsson, K. Domen, M. Antonietti, Nat. Mater. 8 (2009) 76–80.
[6] S.C. Yan, Z.S. Li, Z.G. Zou, Langmuir 25 (2009) 10397–10401.
[7] X. Wang, S. Blechert, M. Antonietti, ACS Catal. 2 (2012) 1596–1606.
[8] Y. Zheng, J. Liu, J. Liang, M. Jaroniecc, S.Z. Qiao, Energy Environ. Sci. 5 (2012) 6717–6731.
[9] H. Xu, J. Yan, Y. Xu, Y. Song, H. Li, J. Xia, C. Huang, H. Wan, Appl. Catal. B: Environ. 129 (2013) 182–193.
[10] Z. Huang, F. Li, B. Chen, T. Lu, Y. Yuan, G. Yuan, Appl. Catal. B: Environ. 136–137 (2013) 269–277.
[11] S. Cao, J. Yu, J. Phys. Chem. Lett. 5 (2014) 2101–2107.
[12] K. Schwinghammer, B. Tuffy, M.B. Mesch, E. Wirnhier, C. Martineau, F. Taulelle, W. Schnick, J. Senker, B.V. Lotsch, Angew. Chem. Int. Ed. 52 (2013) 2435–2439.
[13] J. Hong, X. Xia, Y. Wang, R. Xu, J. Mater. Chem. 22 (2012) 15006–15012.
[14] S.S. Park, S.W. Chu, C. Xue, D. Zhao, C.S. Ha, J. Mater. Chem. 21 (2011) 10801–10807.
[15] J. Zhang, M. Zhang, S. Lin, X. Fu, X. Wang, J. Catal. 310 (2013) 24–30.
[16] J. Zhang, X. Chen, K. Takanabe, K. Maeda, K. Domen, J.D. Epping, X. Fu, M. Antonietti, X. Wang, Angew. Chem. Int. Ed. 49 (2010) 441–444.
[17] T. Tyborski, C. Merschjann, S. Orthmann, F. Yang, M.-C. Lux-Steiner, T. Schedel-Niedrig, J. Phys. Condens. Matter. 24 (2012) 162201.
[18] J. Zhang, J. Sun, K. Maeda, K. Domen, P. Liu, M. Antonietti, X. Fu, X. Wang, Energy Environ. Sci. 4 (2011) 675–678.
[19] A.B. Jorge, D.J. Martin, M.T.S. Dhanoa, A.S. Rahman, N. Makwana, J. Tang, A. Sella, F. Corà, S. Firth, J.A. Darr, P.F. McMillan, J. Phys. Chem. C 117 (2013) 7178–7185.
[20] S. Kumar, T. Surendar, B. Kumar, A. Baruah, V. Shanker, RSC Adv. 4 (2014) 8132–8137.
[21] Y. Zhang, T. Mori, J. Ye, Sci. Adv. Mater. 4 (2012) 282–291.
[22] J. Li, B. Shen, Z. Hong, B. Lin, B. Gao, Y. Chen, Chem. Commun. 48 (2012) 12017–12019.
[23] J. Xu, H.T. Wu, X. Wang, B. Xue, Y.X. Li, Y. Cao, Phys. Chem. Chem. Phys. 15 (2013) 4510–4517.
[24] S. Wang, C. Li, T. Wang, P. Zhang, A. Li, J. Gong, J. Mater. Chem. A 2 (2014) 2885–2890.
[25] Z. Zhang, J. Long, X. Xie, H. Zhuang, Y. Zhou, H. Lin, R. Yuan, W. Dai, Z. Ding, X. Wang, X. Fu, Appl. Catal. A: Gen. 425–426 (2012) 117–124.
[26] B. Jürgens, E. Irran, J. Senker, P. Kroll, H. Müller, W. Schnick, J. Am. Chem. Soc. 125 (2003) 10288–10300.
[27] T. Sano, S. Tsutsui, K. Koike, T. Hirakawa, Y. Teramoto, N. Negishi, K. Takeuchi, J. Mater. Chem. A 1 (2013) 6489–6496.
[28] H. Zhang, A. Yu, J. Phys. Chem. C 118 (2014) 11628–11635.
[29] B. Long, J. Lin, X. Wang, J. Mater. Chem. A 2 (2014) 2942–2951.
[30] M. Shao, L. Cheng, X. Zhang, D.D.D. Ma, S. Lee, J. Am. Chem. Soc. 131 (2009) 17738–17739.